PAPER

Brønsted activity of two-dimensional zeolites compared to bulk materials

Joachim Sauer*

Different reactivity parameters yield different results for the relative acidity of zeolitic Brønsted sites in thin films and in bulk materials. Whereas the adsorption energies of ammonia and pyridine are about the same, the energy of deprotonation is much lower for two-dimensional systems than for three-dimensional systems. It is shown that this is due to the smaller effective dielectric constant of two-dimensional systems, which leads to much lower deprotonation energies, but also to much lower interaction energies between the protonated molecule and the negatively charged surface site. In the total adsorption energies, both effects nearly compensate each other.

1. Introduction

The catalytic activity[1,2] of the proton forms of zeolites originates from bridging Al–O(H)–Si groups which represent Brønsted acid sites.[3,4] They are located at the internal surface of the channels and cavities of the crystalline zeolite structures. In recent years two-dimensional zeolites, *i.e.* nanosheets as thin as single unit cells of, *e.g.* MFI,[5,6] have found much interest.[7] To understand if "being two-dimensional" affects the catalytic activity, we compare the protonation ability of bridging Al–O(H)–Si groups of three-dimensional (3d, bulk) and two-dimensional (2d) zeolites. As a model for the latter, we consider an aluminosilicate bilayer with a two-dimensional arrangement of hexagonal prisms (H-2dH) and compare it with the protonated form of H-chabazite (H-CHA)[8,9] and other zeolites. Such a protonated aluminosilicate bilayer has indeed been grown as an ultra-thin film under UHV conditions by deposition of O_2, Si and Al on the Ru(0001) surface and subsequent adsorption and desorption of water.[8,10] It has also been speculated that low-density large-pore zeolites can be assembled from such double-layer aluminosilicate sheets.[11]

A flat surface may be considered as the limiting case of a pore with an infinitely large curvature. The surface curvature effect of Derouane[12] (Fig. 1) has been invoked to explain the smaller adsorption energies for CO, C_2H_4, and pyridine on the two-dimensional system with a flat surface compared to the microporous bulk systems.[8] If this effect (largely due to dispersion) is approximately eliminated

Humboldt-Universität, Institut für Chemie, Berlin, Germany. E-mail: js@chemie.hu-berlin.de
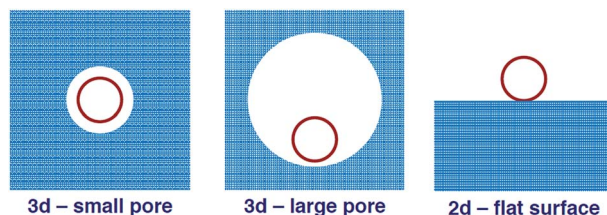
Fig. 1 Worsening of the fit of a molecule (red circle) to the surface from a small pore to a large pore 3d system and to a flat surface.

from the adsorption system, the remaining "specific" interaction is larger for Brønsted sites on the 2d system as compared to the 3d system.[8]

IR spectroscopy has shown that the OH frequency-shifts on adsorption of carbon monoxide and ethene are indeed somewhat larger for the proton forms of aluminosilicate bilayers than for acidic zeolites (H-CHA and H-ZSM-5).[8] Both the 2d and 3d systems are able to protonate ammonia and pyridine.[8] In contrast, much lower deprotonation energies have been obtained for the two-dimensional systems (H-2dH) compared to the bulk system (H-CHA).[9] Hence, the deprotonation energy points to a special effect of being two-dimensional, different from the surface curvature effect, and the question arises: Why is this not seen in the energies of adsorption of ammonia or pyridine that involve proton transfer? Answering this question is the aim of this study.

2. Methods

There are different measures of acidity strength,[13–15] *i.e.* parameters that are related to the (free) energy for the protonation of a substrate molecule S by a zeolitic hydroxyl group ZO–H,

$$Z–OH + S \rightarrow Z–O^{-}\cdots HS^{+}. \tag{1}$$
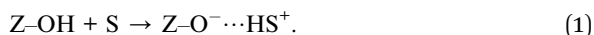
They may be categorized according to different stages of reaction (1), ranging from little mutual perturbation of the reactants ("early" transition state) to completed proton transfer ("late" transition state). Parameters that describe the intrinsic acidity without any interaction with a substrate molecule are the OH frequency[13,16] (lower frequency – weaker OH bond – stronger acid) and the ^{1}H-NMR shift[17,18] (larger shift – more positive charge on proton site – stronger acid) for the initial state, as well as the deprotonation energy (or the proton affinity of the deprotonated Brønsted site) for the final state.[4]

Although the deprotonation energy neglects interactions between the substrate and the catalyst surface, often it predicts reactivity trends correctly. An example is the H-SSZ-13/H-SAPO-34 comparison: two catalysts with the same active site and framework structure (CHA), but with different framework compositions, SiO_2/$AlPO_4$. The calculations yielded deprotonation energies that were, depending on the specific method, 30–40 kJ mol^{-1} higher for H-SAPO-34 than for H-SSZ-13, indicating a lower acidity of the former. This fits the statement "Another key feature of the SAPO-34 molecular sieve is its optimized acidity

relative to aluminosilicate based zeolitic materials" in a publication on the UOP/ hydro methanol-to-olefin process.[19]

The OH frequency shift on adsorption of weak bases such as CO and C_2H_2 is among the parameters that take the interaction with a probe molecule (model substrate) into account and represent an "early" transition state. In contrast, adsorption of strong bases like ammonia or pyridine implies a late transition state with the proton transferred to the reaction partner.

The advantage of a computational approach is that all these parameters can be calculated and their relation can be analysed, see ref. 18, 20 and 21 for comparisons between different parameters. The calculations use density functional theory (DFT) and apply periodic boundary conditions.

The hybrid QM/MM calculations are performed with the B3LYP hybrid functional (QM) and shell-model ion-pair potential for the periodic structure (MM).[22] Harmonic frequencies are calculated for the QM cluster models at the QM:MM structures. They are scaled with a factor of 0.9716, obtained by comparison of the B3LYP frequencies for water and methanol with experimental values.[22] When calculating deprotonation energies, a constant is added to eliminate the effect of different systematic errors in different computational models. Values of -46 and 0 kJ mol^{-1} for Hartree–Fock and DFT (B3LYP) results, respectively, are obtained from calibration calculations for the related molecules methanol and silanol for which very accurate deprotonation energies are known.[9,23] For further details on QM/MM calculations see ref. 9.

Details of the full DFT (PBE functional + dispersion) slab calculations of the interaction of CO, C_2H_4, NH_3, and NC_5H_5 with acidic sites are given in ref. 8. The OH vibrational wavenumbers for the 2dH system have been calculated from the DFT bond distances making use of the ω/r correlation with anharmonicity corrections proposed by Nachtigall.[24]

3. Results and discussion

Table 1 shows the OH stretching frequency of the H-2dH system and compares it with those of other zeolite frameworks. In the CHA and FAU frameworks there is

Table 1 OH stretching frequencies, ν_{OH} (cm^{-1}), both observed and calculated, and calculated deprotonation energies, E_{DP} (kJ mol^{-1})

Zeolite	Site[a]	ν_{OH}, obsd[b]	ν_{OH}, calcd	E_{DP}[f]	E_{DP}[g]
FAU	O1H	3623	3626[c]	1206	1198[h]
MFI	O7–H	3610	3608[c]	1235	
CHA	O1H	3603	3606[c]	1225	1233[i]
FER	O7–H	3609	3598[d]		1218[j]
2dH	O2–H	3594	3600[e]		1069[i]
CHA	O3–H	3579	3588[c]		
FAU	O3–H	3550	3563[c]	1203	

[a] Crystallographic position. [b] See computational articles for original references to experimental results. [c] Ref. 22. [d] Ref. 25. [e] Ref. 9 – the Ru(0001) surface was included in the model. [f] Ref. 26 and 27 – corrected by -46 kJ mol^{-1}, cf. ref. 28. [g] The correction term is zero. [h] Ref. 23 – Al/Si = 1/11 for CHA. [i] Ref. 9 – Al/Si = 1/7 for 2dH, the Ru(0001) surface was not included in the 2dH model. [j] Ref. 25.

only one crystallographic position for substitution of Si by Al, but there are two different oxygen positions at which the protons can sit. This gives rise to a high-frequency and a low-frequency band for H-CHA and H-FAU. Table 1 shows that the result for H-2dH is bracketed by the high- and low-frequencies of H-CHA, which themselves are embraced by the corresponding frequencies for H-FAU. The calculations reproduce the sequence of the experimental frequencies and, on both scales, the H-2dH result is very close to the result for H-ferrierite (H-FER).

Whereas the unperturbed OH group of H-2dH does not show any peculiarity among the zeolitic OH groups, this changes when probe molecules are used. The OH frequency shift measured on adsorption of CO on H-2dH is 379 cm^{-1}, 63 cm^{-1} larger than the shifts for H-CHA.[8] The calculated shift is also larger, but only 23 cm^{-1}.[8] If one uses the relation between frequency shift and deprotonation enthalpy suggested by Paukshtis and Yurchenko,[29,30] these frequency shifts translate into deprotonation enthalpies for H-2dH that are 35 and 12 kJ mol^{-1}, respectively, lower than the values for H-CHA, indicating a higher acidity of the two-dimensional system.[9]

The surprise comes when the deprotonation energy is explicitly calculated. The value for H-2dH is as much as 164 kJ mol^{-1} lower than that for H-CHA (Table 2). Obviously, the correlation between an initial state parameter (OH frequency shift on complex formation with the weak base CO) and a final state parameter (deprotonation energy) breaks down. The exceptionally low value is a true consequence of the low dimensionality of the thin film that results in a much lower effective dielectric constant for the thin film (1.8) than for the bulk material of the same chemical composition (2.9). As a result, in the thin film, the charge created on deprotonation is less screened and better stabilized by electrostatic interactions with the surrounding ions, as illustrated in Fig. 2. The acidity increase will be less strong if the 2d-system is not a free-standing film in vacuum, but a film on a metal substrate,[9] or if the 2d zeolite sheet is not used for gas phase catalysis, but is surrounded by solvent molecules.

Such a high acidity seems to be in contradiction with the protonation ability of Brønsted sites in the H-2dH films. As other zeolites, they are found to protonate NH$_3$ and NC$_5$H$_5$, whereas on adsorption of CO and C$_2$H$_4$ the proton is not transferred.[8] Moreover, when looking at the adsorption energy differences for the

Table 2 Deprotonation energies, ΔE_{DP}, binding energy of a protonated base molecule on the deprotonated zeolite surface, ΔE_{IP}, and energies of adsorption, ΔE_{Ads}

Zeolite	H-CHA		H-2dH		Difference	
$\Delta E_{DP}(ZOH)^a$	1234		1069		−165	
S	NH$_3$	NC$_5$H$_5$	NH$_3$	NC$_5$H$_5$	NH$_3$	NC$_5$H$_5$
$-\Delta E_{PA}(S)^b$	854	929	854	929	854	929
$+\Delta E_{IP}$	−539	−487	−375	−285	163	202
$\Delta E_{Ads}(S)^c$	−159	−182	−160	−145	−2	37
Dispersion^c	−27	−66	−29	−47	+2	19
"Active site"^{d}	−131	−116	−131	−98	0	18

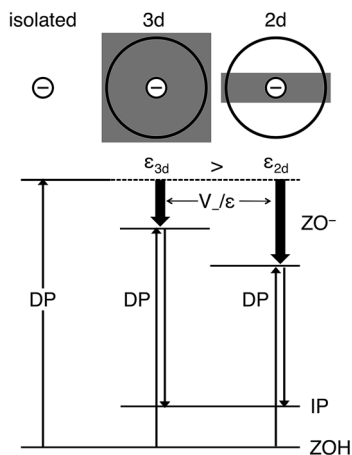^{a} Ref. 9. ^{b} Ref. 31. ^{c} Ref. 8. ^{d} $E_{Ads}(S)$ – dispersion.

Fig. 2 Comparison of deprotonation and ion-pair formation of an isolated site in the gas phase and a site embedded in a three-dimensional (3d) or two-dimensional (2d) dielectric medium. $V\_/\varepsilon$ is the interaction of the negative charge with surrounding charges, ε the effective dielectric constant, DP the deprotonation energy, and IP the ion-pair energy.

molecules that undergo protonation, we find almost no change for NH_3, whereas for NC_5H_5 we find a 37 kJ mol^{-1} less favourable reaction energy on the H-2dH film. We can use the dispersion contribution to the binding energy to estimate the surface curvature effect[12] which yields larger energies for adsorption in a micropore as compared to a flat surface (Table 2). If we remove the dispersion contribution, we will get an interaction energy that relates to the "active site". For NH_3 this parameter does not indicate any difference between the Brønsted site reactivity in a 3d bulk material and a 2d material, while for NC_5H_5 it indicates an even higher activity for the 3d bulk material.

How can this be understood in view of the much lower deprotonation energy of the H-2dH system? The energy of adsorption, ΔE_{Ads}, for the formation of an interacting ion pair (eqn (1)) can be decomposed[27,32] into the energy of the interaction, ΔE_{IP}, between the protonated species and the deprotonated surface site,

$$Z\text{–}O^- + HS^+ \rightarrow Z\text{–}O^- \cdots HS^+ \qquad (2)$$
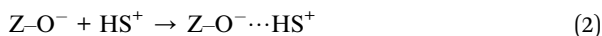
the deprotonation energy, ΔE_{DP}, of the Brønsted site,

$$Z\text{–}OH \rightarrow Z\text{–}O^- + H^+ \qquad (3)$$

and the proton affinity, ΔE_{PA}, of the base molecule

$$S + H^+ \rightarrow HS^+. \qquad (4)$$

Hence,

$$\Delta E_{Ads} = \Delta E_{IP} + \Delta E_{DP} + \Delta E_{PA}. \qquad (5)$$

Table 2 shows the different contributions to ΔE_{Ads}. The ion-pair stabilization ΔE_{IP} is much smaller for the 2d system than for the 3d bulk system. For NH_4^+ formation, the difference of the ion-pair stabilization energies outweighs the difference of the deprotonation energies, whereas for HNC_5H_5 formation, the decrease in ion-pair stabilization (202 kJ mol^{-1}) is even larger than the decrease of the deprotonation energy (165 kJ mol^{-1}). The lower (in absolute terms) ion-pair stabilization energy for 2d systems has the same origin as the lower deprotonation energy: the negative charge in the deprotonated system is more stabilized by surrounding charges if it is less screened (small dielectric constant), and it costs less energy to create it. In turn, less energy is gained when annihilating this charge by ion-pair formation.

For different zeolite structures, it has been shown before that the sequence of deprotonation energies and the sequence of NH_3 adsorption energies is not the same (Table 3).[27] For the four different framework structures, the deprotonation energies vary over 29 kJ mol^{-1} and the ion-pair formation energies over 23 kJ mol^{-1}, whereas the energies of NH_3 adsorption vary over 10 kJ mol^{-1} only. The differences of the ion-pair formation energies partially outweigh differences of the deprotonation energies. This general compensation effect is connected with the properties of conjugated acid–base pairs. The anion Z–O^- formed on deprotonation of a stronger acid Z–OH is a weaker base and, hence, binds the "acid" NH_4^+ less strongly. In addition, there are effects connected with the specific local surface structure around the active site.

For the isomorphous substitution of metal ions into microporous aluminium phosphates (AlPO-34) and chabazite, the trend has been confirmed that NH_3 adsorbs more strongly if the deprotonation energy becomes smaller, but the correlation is not quantitative.[21] Although a good correlation between the heat of NH_3 adsorption and the enthalpy barrier for the methylation of propene could be established,[21] this may not always be the case, for example different reactivity sequences of H-MFI and H-MOR have been predicted if substituted amines and pyridines are used as probe molecules.[33]

4. Conclusions

Calculated deprotonation energies indicate a much higher intrinsic acidity for Brønsted sites in two-dimensional aluminosilicates than in bulk zeolites, whereas the energy of ammonia adsorption shows hardly any difference. The difference between the two reactivity parameters is due to the interaction of the NH_4^+ cation formed on protonation of NH_3 with the negatively charged surface site. The differences of this interaction between the two- and three-dimensional case outweigh the differences in the deprotonation energies.

Table 3 Deprotonation energies, ΔE_{DP}, ion-pair formation energies, ΔE_{IP}, and energies of adsorption of NH_3, ΔE_{Ads}[27]

Zeolite	H-FAU	H-CHA	H-MOR	H-MFI
ΔE_{DP}	1206	1225	1230	1235
ΔE_{IP}	−457	−476	−484	−480
ΔE_{Ads}	−109	−109	−116	−106

Whereas the deprotonation energy is a perfect measure of the intrinsic acidity for gas phase reactions, it is not a suitable reactivity parameter for the design of solid acids.

Acknowledgements

References

1 A. Corma, *Chem. Rev.*, 1995, **95**, 559.
2 A. Corma, *J. Catal.*, 2003, **216**, 298.
3 W. O. Haag, R. M. Lago and P. B. Weisz, *Nature*, 1984, **309**, 589.
4 W. J. Mortier, J. Sauer, J. A. Lercher and H. Noller, *J. Phys. Chem.*, 1984, **88**, 905.
5 M. Choi, K. Na, J. Kim, Y. Sakamoto, O. Terasaki and R. Ryoo, *Nature*, 2009, **461**, 246.
6 Y. Seo, K. Cho, Y. Jung and R. Ryoo, *ACS Catal.*, 2013, **3**, 713.
7 W. J. Roth, P. Nachtigall, R. E. Morris and J. Čejka, *Chem. Rev.*, 2014, **114**, 4807.
8 J. A. Boscoboinik, X. Yu, E. Emmez, B. Yang, S. Shaikhutdinov, F. D. Fischer, J. Sauer and H.-J. Freund, *J. Phys. Chem. C*, 2013, **117**, 13547.
9 M. Rybicki and J. Sauer, *Phys. Chem. Chem. Phys.*, 2015, **17**, 27873.
10 J. A. Boscoboinik, X. Yu, B. Yang, F. D. Fischer, R. Włodarczyk, M. Sierka, S. Shaikhutdinov, J. Sauer and H.-J. Freund, *Angew. Chem., Int. Ed.*, 2012, **51**, 6005.
11 C. J. Dawson, M. A. B. Pope, M. O'Keeffe and M. M. J. Treacy, *Chem. Mater.*, 2013, **25**, 3816.
12 E. G. Derouane, J.-M. Andre and A. A. Lucas, *J. Catal.*, 1988, **110**, 58.
13 J. Sauer, *J. Mol. Catal.*, 1989, **54**, 312.
14 W. E. Farneth and R. J. Gorte, *Chem. Rev.*, 1995, **95**, 615.
15 E. G. Derouane, J. C. Védrine, R. R. Pinto, P. M. Borges, L. Costa, M. A. N. D. A. Lemos, F. Lemos and F. R. Ribeiro, *Catal. Rev. Sci. Eng.*, 2013, **55**, 454.
16 H. Kriegsmann, *Z. Phys. Chem. (Leipzig)*, 1988, **269**, 178.
17 H. Pfeifer, D. Freude and M. Hunger, *Zeolites*, 1985, **5**, 274.
18 U. Fleischer, W. Kutzelnigg, A. Bleiber and J. Sauer, *J. Am. Chem. Soc.*, 1993, **115**, 7833.
19 J. Q. Chen, A. Bozzano, B. Glover, T. Fuglerud and S. Kvisle, *Catal. Today*, 2005, **106**, 103.
20 M. Sierka, U. Eichler, J. Datka and J. Sauer, *J. Phys. Chem. B*, 1998, **102**, 6397.
21 C.-M. Wang, R. Y. Brogaard, B. M. Weckhuysen, J. K. Nørskov and F. Studt, *J. Phys. Chem. Lett.*, 2014, **5**, 1516.
22 M. Sierka and J. Sauer, *J. Phys. Chem. B*, 2001, **105**, 1603.
23 M. Sierka and J. Sauer, *Faraday Discuss.*, 1997, **106**, 41.
24 P. Nachtigall, O. Bludsky, L. Grajciar, D. Nachtigallova, M. R. Delgado and C. O. Arean, *Phys. Chem. Chem. Phys.*, 2009, **11**, 791.
25 V. Nieminen, M. Sierka, D. Y. Murzin and J. Sauer, *J. Catal.*, 2005, **231**, 393.

26 U. Eichler, M. Brändle and J. Sauer, *J. Phys. Chem. B*, 1997, **101**, 10035.

27 M. Brändle and J. Sauer, *J. Am. Chem. Soc.*, 1998, **120**, 1556.

28 J. Sauer, in *Modelling of Structure and Reactivity in Zeolites*, ed. C. R. A. Catlow, Academic Press, London, 1992, p. 183.

29 E. A. Paukshtis, R. I. Soltanov and E. N. Yurchenko, *React. Kinet. Catal. Lett.*, 1981, **16**, 93.

30 E. A. Paukshtis and E. N. Yurchenko, *Russ. Chem. Rev.*, 1983, **52**, 242.

31 E. P. Hunter and S. G. Lias, in *NIST Chemistry WebBook, NIST Standard Reference Database Number 69*, ed. P. J. Linstrom and W. G. Mallard, National Institute of Standards and Technology, Gaithersburg MD, 2005, vol. 20899.

32 M. Brändle and J. Sauer, *J. Mol. Catal. A: Chem.*, 1997, **119**, 19.

33 C. Lee, D. J. Parrillo, R. J. Gorte and W. E. Farneth, *J. Am. Chem. Soc.*, 1996, **118**, 3262.